# Smart Reflector-assisted Alamouti-coded FBMC-OQAM System in LTE Channel Environment

Radhashyam Patra and Arunanshu Mahapatro

***Abstract*—This paper proposes a framework for transmitting Alamouti-coded filter bank multi-carrier offset quadrature amplitude modulated (FBMC-OQAM) signals via smart reflector (SR), a technique for ensuring future-generation wireless communications. The SR consists of several reflecting elements which are tiny, passive, reconfigurable and responsible for intelligently altering the phases of incident signals to cancel out the impairing effects of channel phases. Analytically we derived the phases to be introduced by the SR elements by maximizing the instantaneous-signal-to-noise-ratio (ISNR) at the receiver (Rx). Consequently, system's bit-error-rate (BER) performance is improved. We compared the BER performance of the proposed system with that of the conventional Alamouti-coded FBMC-OQAM system by varying the number of SR elements, considering long-term-evolution (LTE) channel scenarios like Extended Pedestrian-A (EPA), Extended Vehicular-A (EVA), Extended Typical Urban (ETU) and different modulation schemes such as 4QAM, 16QAM, 64QAM, 128QAM and 256QAM. The MATLAB simulation results show that Alamouti-coded FBMC transmission based on SR is a viable option for next-generation wireless communication systems from BER perspective.**

***Index Terms*—FBMC, OQAM, SR, Alamouti-Code, ISNR, BER, LTE, EPA, EVA, ETU, QAM.**

## I. Introduction

Identifying the most appropriate waveform for fulfilling the growing necessity of higher data rate in future generation wireless communication is a fascinating topic. Third generation partnership project (3GPP) considered orthogonal frequency division multiplexing (OFDM) as a candidate waveform for fourth generation (4G) wireless communication because of the following advantages: 1) backward compatibility with 3G and 2G, 2) ease in implementation of OFDM as almost all the computations can be done by fast Fourier transform (FFT) and inverse FFT (IFFT) [1], [2], [3]. However, OFDM system has the following disadvantages: 1) spectral loss because of the cyclic prefix (CP) used for synchronization, 2) high out-of-band (OB) power emission [4], [5], [6], [7], [8]. This motivated the researchers to think of other modulation schemes. Filter bank multicarrier (FBMC) modulation emerged as the front runner among the alternatives to OFDM for future generation communication because of the following reasons: 1) the pulse shaping prototype filters (PFs) used in the FBMC system highly suppresses the OB power emission, 2) highly spectral efficient as no CP is used, 3) flexible time-frequency resource allocation as shown in Fig. 1, 4) well localization in frequency domain [9], [10]. FBMC system also have the disadvantage such as supporting orthogonality only for real symbols which poses extra challenge in channel estimation

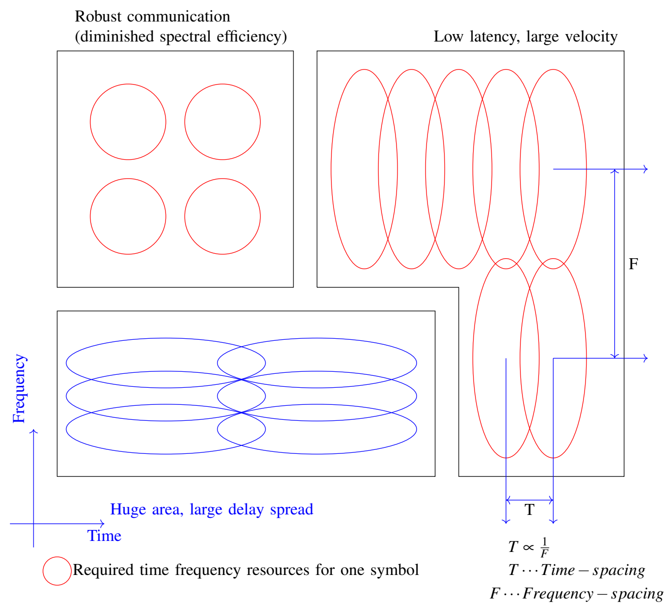


Fig. 1. Flexible time-frequency Resources Allocation.

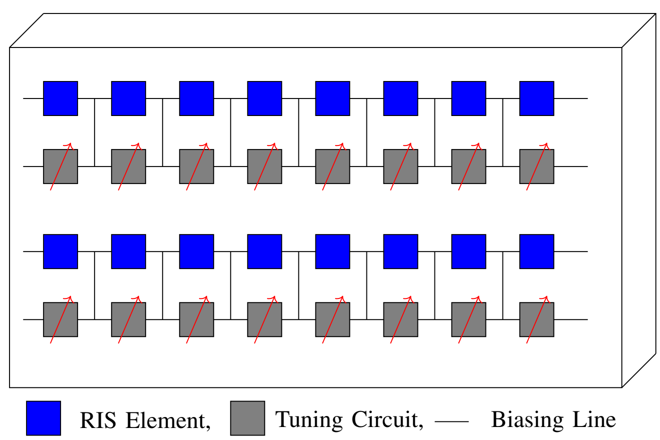


Fig. 2. Conceptual Architecture of an SR

Manuscript received November 27, 2024; revised March 15, 2025.

Radhashyam Patra is an assistant professor in the department of Electronics and Telecommunication Engineering, Veer Surendra Sai University of Technology Burla, Odisha, India, 768018 (Email: radhashyampatra2211@gmail.com).

Arunanshu Mahapatro is an associate professor in the department of Electronics and Telecommunication Engineering, Veer Surendra Sai University of Technology Burla, Odisha, India, 768018 (Email: arun227@gmail.com).

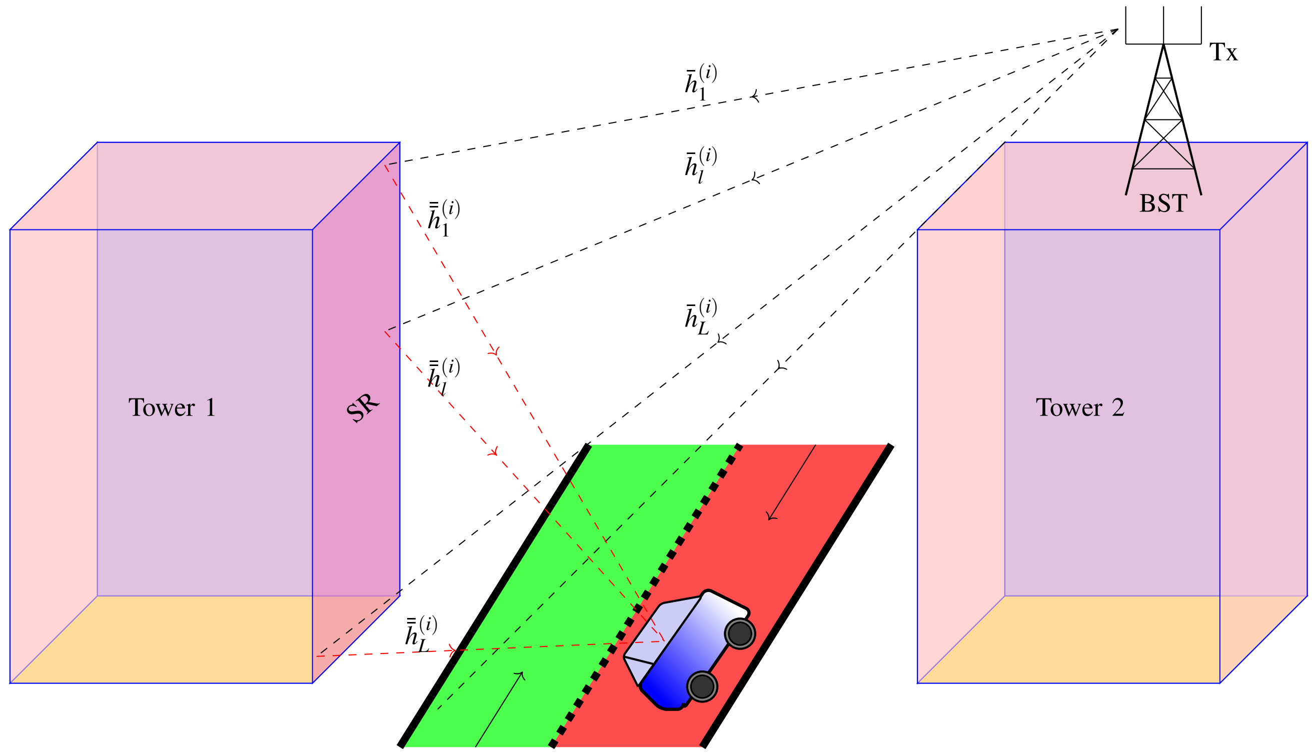


Fig. 3. Practical scenario showing importance of SR-assistance in future generation communication.

[4]. However, this disadvantage is insignificant compared to its advantages. FBMC can be implemented in many forms such as cosine modulated multitone (CMT), filtered multitone (FMT) and offset quadrature amplitude modulation (OQAM). But, FBMC-OQAM is chosen widely as it provides the highest spectral efficiency [11]. Further, to take the advantages of transmission diversity such as the robustness against channel fading, increased reliability and good performance in wireless applications even in low signal-to-noise ratio (SNR), Alamouti-coding [12] is blended with the FBMC-OQAM system in either a time-reversal (TR) [13] or a frequency reversal (FR) [14], [15] manner. The FR method outperforms the TR method from bit-error-rate (BER) perspective [14].

Further, to meet the increasing demands of user for more reliability and higher data rate, research is going on. Propagation control techniques are a solution in this direction and will predominate future wireless communication [16], where the multicarrier translated signal is not sent directly to the channel. Instead, the signal is sent to a smart reflector (SR) (also termed as intelligent reflecting surface (IRS)) and then reflected to the channel. Propagation-controlled communication is especially useful in areas with no line-of-sight (LOS) path between the transmitting and the receiving antennas, such as hilly and high rise urban areas [17]. SR is an almost passive surface consisting of many tiny reconfigurable smart elements [18] as shown in Fig. 2. The term “smart" in this context refers to the passive element’s understanding of the channel phases. The elements are reconfigurable in the sense that the phases they introduce on the incident signal can be changed. The multi-carrier translated signal from the transmitting antenna is incident on the SR, and the SR then adds the required phases to the incident signal to cancel out the impairments caused by the channel (path between the SR and the receiver) phases. This significantly improves the SNR at the receiver. SNR can also be improved by using a power amplifier (PA) before transmission, but this requires a lot of power [19] which is not suitable for energy efficient communication. Also, increasing power increases the peak-to-average-power-ratio (PAPR) of the transmitted signal which needs to be supressed by employing various methods as given in [20]. In contrast, the SR is made up of many compact, inexpensive, and almost passive reflecting elements that reflect only the incident wave with an appropriate phase alteration, requiring far less power than the PA [21], [22], [23], [24]. So, the SR-assisted propagation control technique has superiority over the PA method. SNR can also be improved using hybrid multiple input and multiple output architecture (MIMO). However, in MIMO design multiple antennas are used which process the signal at RF level thus demanding high power. This justifies that SR-assisted system is having preference over MIMO system also.

The authors in [25], [26] incorporated the SR/IRS assisted propagation control in OFDM and FBMC system respectively. This motivated us to incorporate the SR assisted propagation control method in Alamouti-coded FBMC-OQAM system.

This work introduces a novel physical layer communication method for future-generation wireless communication. The major contributions are enlisted below.

1) A novel physical layer is proposed which utilizes FBMC-

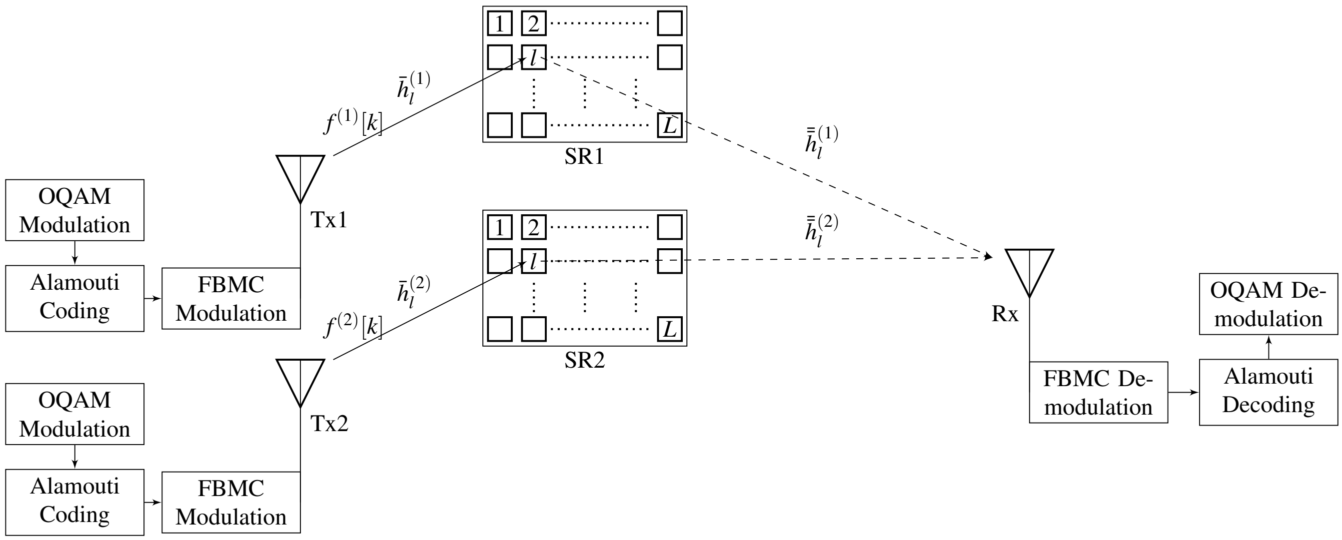


Fig. 4. SR-assisted Alamouti coded FBMC-OQAM System.

| | Code symbols at Tx Antenna 1 i.e., $x^{(1)}_{m,n}$ | | | | | | | | | |
|---|---|---|---|---|---|---|---|---|---|---|
| n \ m | 1 | 2 | $\cdots$ | $\overline{M}/2-1$ | $\overline{M}/2$ | $\overline{M}/2+1$ | $\cdots$ | $\overline{M}-2$ | $\overline{M}-1$ | $\overline{M}$ |
| 1 | $a^{(1)}_{1,1}$ | $a^{(1)}_{2,1}$ | $\cdots$ | $a^{(1)}_{\overline{M}/2-1,1}$ | 0 | $-a^{(2)}_{\overline{M}/2-1,1}$ | $\cdots$ | $-a^{(2)}_{2,1}$ | $-a^{(2)}_{1,1}$ | 0 |
| 2 | $a^{(1)}_{1,2}$ | $a^{(1)}_{2,2}$ | $\cdots$ | $a^{(1)}_{\overline{M}/2-1,2}$ | 0 | $-a^{(2)}_{\overline{M}/2-1,1}$ | $\cdots$ | $-a^{(2)}_{2,1}$ | $-a^{(2)}_{1,1}$ | 0 |
| $\vdots$ | $\vdots$ | $\vdots$ | $\vdots$ | $\vdots$ | $\vdots$ | $\vdots$ | $\vdots$ | $\vdots$ | $\vdots$ | $\vdots$ |

| | Code symbols at Tx Antenna 2 i.e., $x^{(2)}_{m,n}$ | | | | | | | | | |
|---|---|---|---|---|---|---|---|---|---|---|
| n \ m | 1 | 2 | $\cdots$ | $\overline{M}/2-1$ | $\overline{M}/2$ | $\overline{M}/2+1$ | $\cdots$ | $\overline{M}-2$ | $\overline{M}-1$ | $\overline{M}$ |
| 1 | $a^{(2)}_{1,1}$ | $a^{(2)}_{2,1}$ | $\cdots$ | $a^{(2)}_{\overline{M}/2-1,1}$ | 0 | $a^{(1)}_{\overline{M}/2-1,1}$ | $\cdots$ | $a^{(1)}_{2,1}$ | $a^{(1)}_{1,1}$ | 0 |
| 2 | $a^{(2)}_{1,2}$ | $a^{(2)}_{2,2}$ | $\cdots$ | $a^{(2)}_{\overline{M}/2-1,2}$ | 0 | $a^{(1)}_{\overline{M}/2-1,1}$ | $\cdots$ | $a^{(1)}_{2,1}$ | $a^{(1)}_{1,1}$ | 0 |
| $\vdots$ | $\vdots$ | $\vdots$ | $\vdots$ | $\vdots$ | $\vdots$ | $\vdots$ | $\vdots$ | $\vdots$ | $\vdots$ | $\vdots$ |

Fig. 5. Frequency Reversed Alamouti coding

OQAM for modulation, Alamouti-coding for transmission diversity and SR for signal propagation control.

2) We derived the analytical optimum phase values required for maximizing the received signal ISNR.
3) Through MATLAB simulation, we demonstrated improved BER performance in comparison with conventional Alamouti-coded FBMC-OQAM systems for channel models like Extended Pedestrian-A (EPA), Extended Vehicular-A (EVA) and Extended Typical Urban (ETU) [27], [28] for different QAM modulation schemes.

The remainder of the paper is arranged as follows. Section II elaborates the proposed system architecture that includes the design of FR Alamouti-coded FBMC-OQAM system, smart reflector incorporation in the system. Section III describes the derivation of the analytical optimum values of the phases of the SR elements. The MATLAB simulation outputs are presented in Section IV and the conclusions are drawn in Section V.

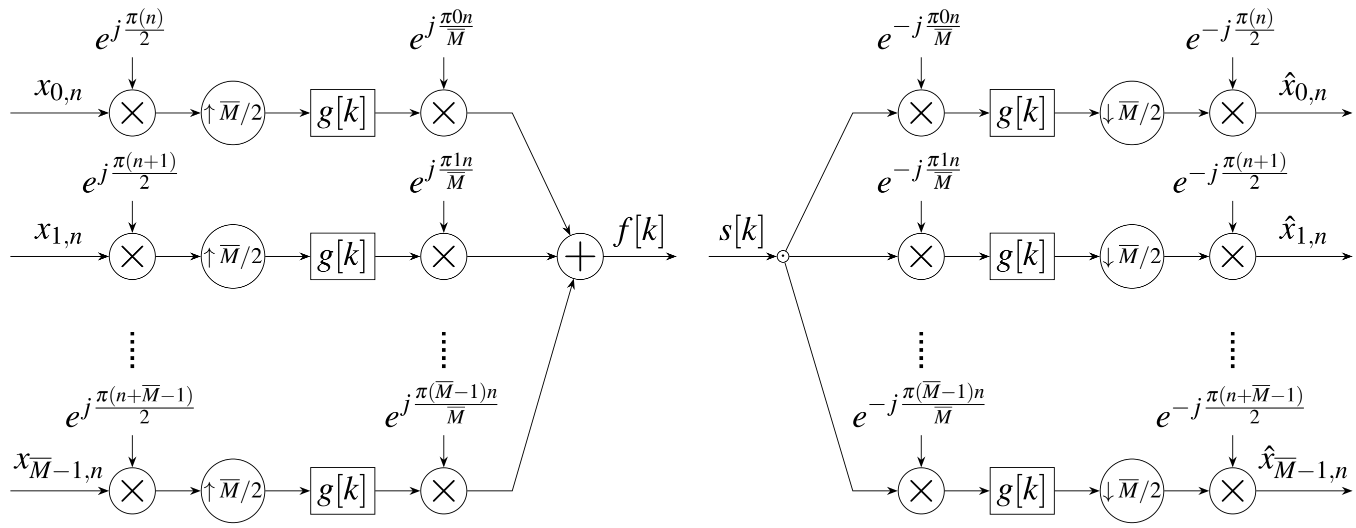


Fig. 6. FBMC-OQAM Transceiver System.

## II. SYSTEM ARCHITECTURE

In this section we explain the practical wireless communication scenario where SR-assistance is extremely useful, the proposed transmitter architecture, SR channel modeling, the proposed receiver architecture and lastly the step-by-step processes involved in the entire system in sequel.

### *A. Practical Wireless Communication Scenario Considered*

The practical scenario which is considered in this work is depicted in Fig. 3 where the antenna inside the vehicle in motion on the road is not receiving or transmitting minimum power to continue the communication with the base station (BST) mounted on the Tower 2. In-order-to address such practical issues, a SR is placed on the wall of another tower strategically that will have LOS communication with the BST and reflects the incident waves on it towards the road.

### *B. Proposed Transmitter Architecture*

The proposed physical layer i.e. SR-assisted Alamouti-coded FBMC-OQAM system model is depicted in Figure 4. It is considered that the BST and SR are stationary and having LOS connection with BST and the user is in motion.

The complex QAM symbols for Tx1 and Tx2 are represented by $c^{(1)}_{m,n}$ and $c^{(2)}_{m,n}$ where $m,n$ represents the frequency and time index respectively. The complex QAM symbols $c^{(i)}_{m,n}$ are converted into real symbols $a^{(i)}_{m,n}$ as per OQAM principle and is given by [4]:

$$a^{(i)}_{m,2n} = \begin{cases} \Re(c^{(i)}_{m,n}), & m \text{ even} \\ \Im(c^{(i)}_{m,n}), & m \text{ odd} \end{cases} ;$$
$$a^{(i)}_{m,2n+1} = \begin{cases} \Im(c^{(i)}_{m,n}), & m \text{ even} \\ \Re(c^{(i)}_{m,n}), & m \text{ odd} \end{cases} , \tag{1}$$

where $(i)$ corresponds to the transmitter number $1,2$, $\Re(\cdot)$ and $\Im(\cdot)$ correspond to real and imaginary part respectively.

Now, these real OQAM symbols are used for generation of Alamouti-code pairs for FBMC modulation. The total number of sub-carriers considered is $M$ and is divided into many blocks, each with $\overline{M}$ sub-carriers. Figure 5 shows how each block is integrated independently. Each block consists of two half blocks with a single zero (null) after each $\overline{M}/2-1$ symbol. The real OQAM symbols are situated in the left half-block and the corresponding Alamouti-coded symbols are positioned in the right half-block in a frequency-reversing way. Between the blocks, the null sub-carriers cause the blocks to become mutually orthogonal.

In the sub-carrier-time frame, the real OQAM symbol couplet $(a^{(1)}_{m,n}, a^{(2)}_{m,n})$ will be broadcasted after Alamouti-coded at $(m,n)$th and $(\overline{M}-m,\overline{M})$th slots. Transmitters Tx1 and Tx2 broadcast the Alamouti coded symbols $x^{(1)}_{m,n}$ and $x^{(2)}_{m,n}$ at the $(m,n)$th slot of the subcarrier-time matrix. Consequently, the Alamouti-code frame is formed by the coded symbol couplets in the frequency reversal places at each transmitter, which are $(x^{(1)}_{m,n}, x^{(1)}_{\overline{M}-m,n})$ and $(x^{(2)}_{m,n}, x^{(2)}_{\overline{M}-m,n})$ and is given by [14]:

$$\begin{pmatrix} x^{(1)}_{m,n} & x^{(1)}_{\overline{M}-m,n} \\ x^{(2)}_{m,n} & x^{(2)}_{\overline{M}-m,n} \end{pmatrix} = \begin{pmatrix} a^{(1)}_{m,n} & -a^{(2)}_{m,n} \\ a^{(2)}_{m,n} & a^{(1)}_{m,n} \end{pmatrix}. \tag{2}$$

Additionally, the signal emitted from $i$th transmitter is in accordance with the FBMC modulation scheme which is shown in Figure 6 and is given by [4]:

$$f^{(i)}[k] = \sum_{p=1}^{\overline{M}-1} \sum_{q=-\infty}^{\infty} x^{(i)}_{p,q} \chi_{p,q} g[k - \frac{Tq}{2}] e^{j\frac{2\pi pk}{T}}, \tag{3}$$

where $g[k]$ represents a PF with unit energy and good frequency localization, such as the PHYDYAS filter [29], and $T$ represents the QAM symbol period. For $1 \leq p \leq \overline{M}/2-1$, the phase alteration needed to transform the real symbols $x^{(1)}_{p,q}$

and $x_{p,q}^{(2)}$ into OQAM symbols in the left half sub-block is represented by $\chi_{p,q}$ and is given by:

$$\chi_{p,q} = \begin{cases} 1 \text{ or } -1 \text{ for even } p+q \\ j \text{ or } -j \text{ for odd } p+q \end{cases}. \quad (4)$$

However, phase shift required in the right half sub-block, i.e., $\chi_{\overline{M}-p,q}$ for $1 \leq p \leq \overline{M}/2-1$ is given by:

$$\chi_{\overline{M}-p,q} = \chi_{p,q}^{*}. \quad (5)$$

Next, we describe the incorporation of the smart reflector with the system.

*C. SR Channel Modeling*

Instead of transmitting the modulated signals $f^{(1)}[k]$, $f^{(2)}[k]$ directly to the channel, these are sent to the corresponding SR. Then the reflected signals from SRs are sent to the channel and then received at the receiver as shown in Figure 4. Similar to reference [16], we assume that no LOS path exists between the Txs and the Rx. Since the SR and the Tx are considered as stationary and having LOS link, the channel between the Txs and the $l$th element of SR is modeled as one-tap flat-fading channel i.e. Gaussian channel with mean zero and variance one and is expressed by:

$$\bar{h}_l^{(i)} = \bar{\beta}_l^{(i)} e^{-j\bar{\psi}_l^{(i)}}, \quad (6)$$

where $\bar{\beta}_l^{(i)}$ is the magnitude and $-\bar{\psi}_l^{(i)}$ is the phase. Both the real and imaginary parts of $\bar{h}_l^{(i)}$ are having Gaussian distribution with $\mathcal{N}(0,1)$. Therefore, $\bar{\psi}_l^{(i)}$ is uniformly distributed over $[0,2\pi]$. Each SR consists of $L$ passive reflecting elements in the 2-dimensional array. The channel between the $l$th reflecting element of $i$th SR and the Rx is modeled as:

$$\bar{\bar{h}}_l^{(i)} = \bar{\bar{\beta}}_l^{(i)} e^{-j\bar{\bar{\psi}}_l^{(i)}}, \quad (7)$$

where $i = 1,2$, $l = \{1,\cdots,L\}$, $\bar{\bar{\beta}}_l^{(i)}$ is the magnitude and $-\bar{\bar{\psi}}_l^{(i)}$ is the phase. Both the real and imaginary parts of $\bar{\bar{h}}_l^{(i)}$ are having Gaussian distribution with $\mathcal{N}(0,1)$. Therefore, $\bar{\bar{\psi}}_l^{(i)}$ is uniformly distributed over $[0,2\pi]$. Therefore, the resultant channel model $h_l^{(i)}$ can be found by convolution of $\bar{h}^{(i)}$ and $\bar{\bar{h}}_l^{(i)}$ and is expressed by:

$$h_l^{(i)} = \bar{h}_l^{(i)} * \bar{\bar{h}}_l^{(i)} \quad (8)$$

$$\Longrightarrow \beta_l^{(i)} e^{-j\psi_l^{(i)}} = \bar{\beta}_l^{(i)} \bar{\bar{\beta}}_l^{(i)} e^{-j(\bar{\psi}_l^{(i)}+\bar{\bar{\psi}}_l^{(i)})}, \quad (9)$$

where $\beta_l^{(i)} = \bar{\beta}_l^{(i)}\bar{\bar{\beta}}_l^{(i)}$ and $\psi_l^{(i)} = \bar{\psi}_l^{(i)} + \bar{\bar{\psi}}_l^{(i)}$ are the magnitude and the phase of the resultant channel between the BST and the user and $\psi_l^{(i)}$ is uniformly distributed over $[0,2\pi]$. The $l$th element of $i$th SR introduces a phase shift of $\phi_l^{(i)}$ to the incident signal in-order-to nullify the effects of channel phases [16]. In this work we assume that the channel phases are known to the SR elements. However, in practical scenario channel is estimated in the receiver using advanced methods such as optimization algorithms [30], neural network [31], deep learning [32], machine learning [33] etc. Next, we elaborate the successive processing of the received signal at the receiver.

*D. Proposed Receiver Architecture*

The signal received for the block under consideration is provided by:

$$\begin{aligned} s[k] &= \left\{\sum_{l=1}^{L} h_l^{(1)} e^{j\phi_l^{(1)}}\right\} f^{(1)}[k] + \left\{\sum_{l=1}^{L} h_l^{(2)} e^{j\phi_l^{(2)}}\right\} f^{(2)}[k] \\ &\quad +\eta[k] \\ &= \acute{h}^{(1)} f^{(1)}[k] + \acute{h}^{(2)} f^{(2)}[k] + \eta[k], \end{aligned} \quad (10)$$

where $\acute{h}^{(i)} = \left\{\sum_{l=1}^{L} h_l^{(i)} e^{j\phi_l^{(i)}}\right\}$. The received sample $s_{m,n}$ at $(m,n)$th frequency-time slot is obtained after FBMC demodulation and is as expressed below:

$$s_{m,n} = \sum_{k=-\infty}^{+\infty} s[k]\chi_{m,n}^{*} g[k-nT/2] e^{-j\frac{2\pi mk}{T}}, \quad (11)$$

After combined in the receiver, the decision variables $d_{m,n}^{(1)}$ and $d_{m,,n}^{(2)}$ for the data symbols $a_{m,n}^{(1)}$ and $a_{m,,n}^{(2)}$ are formulated as:

$$\begin{aligned} d_{m,n}^{(1)} &= \Re\left[\acute{h}^{(1)*} s_{m,n} + \acute{h}^{(2)} s_{\overline{M}-m,n}^{*}\right], \\ d_{m,n}^{(2)} &= \Re\left[\acute{h}^{(2)*} s_{m,n} - \acute{h}^{(1)} s_{\overline{M}-m,n}^{*}\right], \end{aligned} \quad (12)$$

where $(\cdot)^{*}$ represents the complex conjugate. By substituting (3) into (10) and then into (11), $s_{m,n}$ can be rewritten as:

$$\begin{aligned} s_{m,n} &= \acute{h}^{(1)} \sum_{p=-P}^{P} \sum_{q=-Q}^{Q} \Gamma_{p,q} \chi_{m+p,n+q} \chi_{m,n}^{*} (-1)^{np} x_{m+p,n+q}^{(1)} \\ &\quad + \acute{h}^{(2)} \sum_{p=-P}^{P} \sum_{q=-Q}^{Q} \Gamma_{p,q} \chi_{m+p,n+q} \chi_{m,n}^{*} (-1)^{np} x_{m+p,n+q}^{(2)} \\ &\quad +\eta_{m,n}, \end{aligned} \quad (13)$$

where $\Gamma_{p,q} = \sum_{k=-\infty}^{\infty} g[k-Tq/2] g[k] e^{-j\frac{2\pi pk}{T}}$ and $\eta_{m,n}$ represents the corresponding noise term. The trans-multiplexer output of the PF is also referred to as $\Gamma_{p,q}$. The pulse $g[k]$ is well localized in the frequency and time domain in the FBMC system. For $|p| > P$ or $|q| > Q$, $\Gamma_{p,q}$ thus approximates zero. For this reason, $-P \leq p \leq P$ and $-Q \leq q \leq Q$ are the only summation ranges in (13). Thus, the total interference of the symbol at $(m+p,n+q)$th frequency-time slot to the symbol at $(m,n)$th frequency-time slot can be defined as:

$$\Gamma_{p,q}^{(m,n)} \triangleq \Gamma_{p,q} \chi_{m+p,n+q} \chi_{m,n}^{*} (-1)^{np}. \quad (14)$$

The FBMC property and the PF allow for the deduction of the following properties [4].

**Property I:** $\Gamma_{p,q}^{(m,n)} = \delta_p \delta_q$;

**Property II:** $\Gamma_{-p,q}^{(\overline{M}-m,n)} = \Gamma_{p,q}^{*(m,n)}$

By using (2) and (14) into (13), we obtain:

$$\begin{aligned} s_{m,n} &= \acute{h}^{(1)} \underbrace{\sum_{p=-P}^{P} \sum_{q=-Q}^{Q} \Gamma_{p,q}^{(m,n)} a_{m+p,n+q}^{(1)}}_{\triangleq A} + \\ &\quad \acute{h}^{(2)} \underbrace{\sum_{p=-P}^{P} \sum_{q=-Q}^{Q} \Gamma_{p,q}^{(m,n)} a_{m+p,n+q}^{(2)}}_{\triangleq B} + \eta_{m,n}, \end{aligned} \quad (15)$$

$$s_{\overline{M}-m,n} = \underbrace{\acute{h}^{(1)} \sum_{p=-P}^{P} \sum_{q=-Q}^{Q} \Gamma_{p,q}^{(\overline{M}-m,n)} (-a_{m-p,n+q}^{(2)})}_{\triangleq C} + \underbrace{\acute{h}^{(2)} \Sigma_{p=-P}^{P} \sum_{q=-Q}^{Q} \Gamma_{p,q}^{(\overline{M}-m,n)} a_{m-p,n+q}^{(1)}}_{\triangleq D} + \eta_{\overline{M}-m,n}. \quad (16)$$

Using (15) and (16) in (12), we can write:

$$\begin{aligned} d_{m,n}^{(1)} &= \Re\left[\acute{h}^{(1)*}(\acute{h}^{(1)}A + \acute{h}^{(2)}B) + \acute{h}^{(2)}(\acute{h}^{(1)}C + \acute{h}^{(2)}D)^*\right] \\ &\quad + n_{m,n}^{(1)} \\ &= |\acute{h}^{(1)}|^2 \Re[A] + |\acute{h}^{(2)}|^2 \Re[D^*] + \Re[\acute{h}^{(1)*}\acute{h}^{(2)}(B + C^*)] \\ &\quad + n_{m,n}^{(1)}, \end{aligned} \quad (17)$$

where $n_{m,n}^{(1)} = \Re[\acute{h}^{(1)*}\eta_{m,n} + \acute{h}^{(2)}\eta_{\overline{M}-m,n}^*]$ represents the noise part in $d_{m,n}^{(1)}$. Using property I, $\Re[A]$ can be expressed as given below:

$$\Re[A] = \sum_{p=-P}^{P} \sum_{q=-Q}^{Q} \delta_p \delta_q a_{m+p,n+q} = a_{m,n}^{(1)}. \quad (18)$$

And similarly,

$$\Re[D^*] = a_{m,n}^{(1)}. \quad (19)$$

$C^*$ can be written as:

$$C^* = [\sum_{p=-P}^{P} \sum_{q=-Q}^{Q} \Gamma_{-p,q}^{(\overline{M}-m,n)} (-a_{m+p,n+q}^{(2)})]^*. \quad (20)$$

Using Property II, we get:

$$\begin{aligned} C^* &= [\sum_{p=-P}^{P} \sum_{q=-Q}^{Q} \Gamma_{p,q}^{*(m,n)} (-a_{m+p,n+q}^{(2)})]^* \\ &= -[\sum_{p=-P}^{P} \sum_{q=-Q}^{Q} \Gamma_{p,q}^{(m,n)} (a_{m+p,n+q}^{(2)})] \\ &= -B. \end{aligned} \quad (21)$$

Therefore, using (18), (19), (20) and (21) into (17), we get:

$$d_{m,n}^{(1)} = \left(|\acute{h}^{(1)}|^2 + |\acute{h}^{(2)}|^2\right) a_{m,n}^{(1)} + n_{m,n}^{(1)}. \quad (22)$$

Similarly,

$$d_{m,n}^{(2)} = \left(|\acute{h}^{(1)}|^2 + |\acute{h}^{(2)}|^2\right) a_{m,n}^{(2)} + n_{m,n}^{(2)}, \quad (23)$$

where $n_{m,n}^{(2)}$ represents the noise in $d_{m,n}^{(2)}$. After normalizing (23) we get the detected real OQAM symbols as follows:

$$\begin{aligned} \hat{a}_{m,n}^{(1)} &= a_{m,n}^{(1)} + \frac{n_{m,n}^{(1)}}{\left(|\acute{h}^{(1)}|^2 + |\acute{h}^{(2)}|^2\right)}; \\ \hat{a}_{m,n}^{(2)} &= a_{m,n}^{(2)} + \frac{n_{m,n}^{(2)}}{\left(|\acute{h}^{(1)}|^2 + |\acute{h}^{(2)}|^2\right)}. \end{aligned} \quad (24)$$

The complex constellation points $\hat{c}_{m,n}^{(i)}$ can now be produced by processing $\hat{a}_{m,n}^{(i)}$ as follows [4].

$$\hat{c}_{m,n}^{(i)} = \begin{cases} \hat{a}_{m,n}^{(i)} + j\hat{a}_{m,2n+1}^{(i)} & \text{if } m \text{ even} \\ \hat{a}_{m,2n+1}^{(i)} + j\hat{a}_{m,2n}^{(i)} & \text{if } m \text{ odd} \end{cases}. \quad (25)$$

Next, by performing QAM demodulation on $\hat{c}_{m,n}^{(i)}$, the actual data bits are retrieved.

### *E. Step-by-step Processes Involved in the Proposed System*

1) Two data streams are generated for the transmitter 1 (Tx1) and transmitter 2 (Tx2) and then QAM modulated to obtain the complex QAM sysmbols.
2) The real OQAM symbols are extracted from the complex QAM symbols, and then the Alamouti-code pairs are generated for the Tx1 and Tx2.
3) The pairs are FBMC modulated and transmitted to the SR surfaces, which are composed of several tiny surfaces that reflect the incoming signal while introducing certain phases to it.
4) Then the reflected signals from SRs are sent to the channel and then received at the Rx.
5) The signal at Rx is combined and then FBMC demodulated and then Alamouti-decoded to detect the real OQAM symbols.
6) Then the detected real OQAM symbols are combined to get the complex QAM symbols and then the data stream is detected after QAM demodulation.

Next, we derive the optimum phase values of the SR elements that maximizes the received SNR.

## III. Analytical Optimization of the Phases of the SR Elements

The detection of real OQAM sysmbols expressed in (24) will be best when $\left(|\acute{h}^{(1)}|^2 + |\acute{h}^{(2)}|^2\right)$ is maximum i.e. each $|\acute{h}^{(i)}|^2$ is maximum. Now using (8) and (9) in $\acute{h}^{(i)}$ of (10) we can express $|\acute{h}^{(i)}|^2$ as follows:

$$\begin{aligned} |\acute{h}^{(i)}|^2 &= |\sum_{l=1}^{L} h_l^{(i)} e^{j\phi_l^{(i)}}|^2 \\ &= |\sum_{l=1}^{L} \beta_l^{(i)} e^{j(\phi_l^{(i)} - \psi_l^{(i)})}|^2 \\ &= |\sum_{l=1}^{L} \beta_l^{(i)} e^{j\theta_l^{(i)}}|^2 \\ &= \sum_{l=1}^{L} \{\beta_l^{(i)}\}^2 + 2\sum_{l=1}^{L} \sum_{k=l+1}^{L} \beta_l^{(i)} \beta_k^{(i)} cos(\theta_l^{(i)} - \theta_k^{(i)}), \end{aligned} \quad (26)$$

where $\theta_l^{(i)} = \phi_l^{(i)} - \psi_l^{(i)}$. We know (26) will be maximum when $\theta_l^{(i)} - \theta_k^{(i)} = 0$ i.e. $\theta_l^{(i)} = \theta_k^{(i)} = \theta^{(i)}$. Later we will prove that the SNR of the received signal $s[k]$ will be maximum when this $\theta^{(i)} = 0$ i.e. $\phi_l^{(i)} = \psi_l^{(i)}$.

In this section, firstly we derive the SNR of the received signal $s[k]$ in (10), and next we derive the optimal values

TABLE I
LTE CHANNEL SPECIFICATIONS CONSIDERED [27], [28].

| Channel Models | Parameters | | |
|---|---|---|---|
| | No. of paths | Delay (ns) | Relative Power (dB) |
| EPA | 7 | [0 30 70 90 110 190 410] | [0 -1 -2 -3 -8 -17.2 -20.8] |
| EVA | 9 | [0 30 150 310 370 710 1090 1730 2510] | [0 -1.5 -1.4 -3.6 -0.6 -9.1 -7.0 -12.0 -16.9] |
| ETU | 9 | [0 50 120 200 230 500 1600 2300 5000] | [-1 -1 -1 0 0 0 -3 -5 -7] |

TABLE II
BER COMPARISON OF SR-ASSISTED ALAMOUTI-CODED FBMC-OQAM SYSTEM WITH CONVENTIONAL SYSTEM FOR 64 QAM

| | EPA | | EVA | | ETU | |
|---|---|---|---|---|---|---|
| $E_b/N_0 \rightarrow$ | $-10$dB | 10dB | $-10$dB | 10dB | $-10$dB | 10dB |
| Conventional | $3.2\times10^{-1}$ | $3.3\times10^{-3}$ | $3.6\times10^{-1}$ | $6.4\times10^{-2}$ | $4.0\times10^{-1}$ | $1.5\times10^{-1}$ |
| SR-assisted $L=2$ | $1.4\times10^{-1}$ | $3.4\times10^{-3}$ | $2.4\times10^{-1}$ | $4.0\times10^{-2}$ | $2.8\times10^{-1}$ | $8.9\times10^{-2}$ |
| SR-assisted $L=4$ | $2.5\times10^{-2}$ | $2.7\times10^{-3}$ | $1.2\times10^{-1}$ | $3.4\times10^{-2}$ | $1.6\times10^{-1}$ | $8.2\times10^{-2}$ |
| SR-assisted $L=8$ | $3.2\times10^{-3}$ | $2.4\times10^{-3}$ | $4.8\times10^{-2}$ | $3.4\times10^{-2}$ | $1.0\times10^{-1}$ | $8.2\times10^{-2}$ |
| SR-assisted $L=16$ | $3.2\times10^{-3}$ | $2.4\times10^{-3}$ | $3.6\times10^{-2}$ | $3.4\times10^{-2}$ | $9.0\times10^{-2}$ | $8.2\times10^{-2}$ |

TABLE III
PARAMETERS CONSIDERED IN SIMULATION.

| Parameters | Values |
|---|---|
| Number of sub-carriers in each Tx $M$ | 256 |
| Number of sub-carriers in each block $\bar{M}$ | 32 |
| sub-carrier spacing $\Delta f$ | 15 kHz |
| Number of elements in the SR $L$ | $\{2,4,8,16\}$ |
| $P$ | 1 |
| $Q$ | 3 |
| Total number of Txs | 2 |
| Total number of Rx | 1 |
| Modulation schemes | 4, 16, 64, 128, 256 QAM |
| Channel between SR and user | EPA, EVA, ETU |
| Channel between BST and SR | Flat-fading |
| Pulse shaping PF | Bellanger's PHYDYAS |
| Overlapping factor | 4 |
| Noise | AWGN |
| symbol to noise PSD ratio ($E_b/N_0$) | [-50,10]dB |
| Computer Simulation | MATLAB |

of phases by maximizing this SNR. The transmitted symbols $f^{(i)}[k]$ are amplified by a factor $\sum_{l=1}^{L}\beta_l^{(i)}e^{-j(\psi_l^{(i)}-\phi_l^{(i)})}$ which arises due to the presence of SR elements. The SNR of $s[k]$ is given in (27), where $f^{(1)}[k], f^{(2)}[k], \beta_l^{(1))}, \beta_l^{(2)}, \psi_l^{(1)}$ and $\psi_l^{(2)}$ are statistically independent.

Therefore, the SNR in (27) will be maximum when $\psi_l^{(1)} - \phi_l^{(1)} = 0$, i.e, $\psi_l^{(1)} = \phi_l^{(1)}$ and similarly $\psi_l^{(2)} = \phi_l^{(2)}$. Therefore, the condition for the SNR to be maximum is $\psi_l^{(i)} = \phi_l^{(i)}$ i.e., $\phi_l^{(i)} = -(-\psi_l^{(i)})$. This means the optimal value of the phase $\phi_l^{(i)}$ introduced by the $l$th element of $i$th SR is same as $-\psi_l^{(i)}$ (same in magnitude and opposite in polarity) which is phase of the channel between the $l$th element of $i$th SR and the receiver. In this article, it is considered that the reflecting surface is smart, therefore, the surface has the prior knowledge of the phase of the channel $-\psi_l^{(i)}$. Based on the channel phase, the surface makes the phases introduced by its elements $\phi_l^{(i)}$ equal and opposite in polarity to $-\psi_l^{(i)}$. Hence, the term $\acute{h}^{(i)} = \sum_{l=1}^{L}\beta_l^{(i)}e^{-j(\psi_l^{(i)}-\phi_l^{(i)})}$ in (10) becomes real and can be expressed as:

$$\sum_{l=1}^{L}\beta_l^{(i)}e^{-j(\psi_l^{(i)}-\phi_l^{(i)})} = \sum_{l=1}^{L}\beta_l^{(i)} = \gamma^{(i)}, \tag{28}$$

where $\gamma^{(i)}$ is a real constant. Therefore, (10) can be rewritten as:

$$s[k] = \gamma^{(1)}f^{(1)}[k] + \gamma^{(2)}f^{(2)}[k] + \eta[k]. \tag{29}$$

The SR contributes the component $\gamma^{(i)}$ in (29), which improves the SNR in the SR aided Alamouti coded FBMC-OQAM system (since $\gamma > 1$). Assuming $\gamma^{(1)} = \gamma^{(2)} = \gamma$, power of $f^{(1)}[k]$ and $f^{(2)}[k]$ are same and is $\sigma_f^2$ for all sample instants $k$ and the noise power is $\sigma_\eta^2$, then the effective SNR can be expressed as:

$$\begin{aligned} \mathrm{SNR}_{\mathrm{eff}}^{\text{SR-Ala-FBMC}} &= \frac{|\gamma^{(1)}f^{(1)}[k]|^2 + |\gamma^{(2)}f^{(2)}[k]|^2}{|\eta[k]|^2} \\ &= \frac{2\gamma^2\sigma_f^2}{\sigma_\eta^2}. \end{aligned} \tag{30}$$

However, the conventional Alamouti coded FBMC system has the SNR:

$$\mathrm{SNR}_{\mathrm{eff}}^{\text{Conv-Ala-FBMC}} = \frac{2\sigma_f^2}{\sigma_\eta^2}. \tag{31}$$

We now observe from (30) and (31) that the effective SNR of the SR assisted Alamouti coded FBMC systems is greater than that of the conventional Alamouti coded FBMC systems by a factor of $\gamma^2$. Next, we present the computer simulation for a set of parameters.

$$\begin{aligned}\text{SNR} &= \frac{|\sum_{l=1}^{L}\beta_l^{(1)}exp\{-j(\psi_l^{(1)}-\phi_l^{(1)})\}f^{(1)}[k]+\sum_{l=1}^{L}\beta_l^{(2)}exp\{-j(\psi_l^{(2)}-\phi_l^{(2)})\}f^{(2)}[k]|^2}{|\eta[k]|^2} \\ &= \frac{|\sum_{l=1}^{L}\beta_l^{(1)}exp\{-j(\psi_l^{(1)}-\phi_l^{(1)})\}f^{(1)}[k]|^2+|\sum_{l=1}^{L}\beta_l^{(2)}exp\{-j(\psi_l^{(2)}-\phi_l^{(2)})\}f^{(2)}[k]|^2}{|\eta[k]|^2},\end{aligned} \tag{27}$$

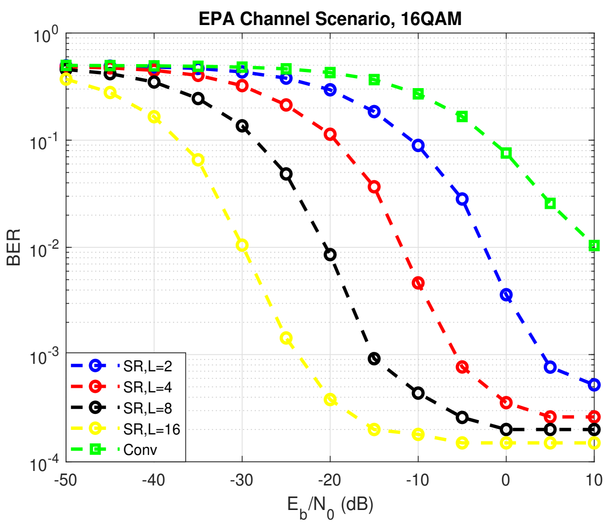


Fig. 7. BER Comparison for different $L$ with EPA Channel, 16QAM modulation.

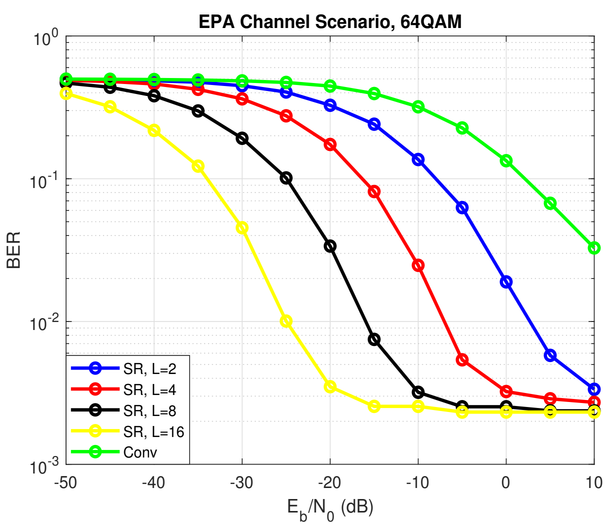


Fig. 8. BER Comparison for different $L$ with EPA Channel, 64QAM modulation.

## IV. SIMULATION RESULTS

The parameters considered in the simulation environment are presented in Table III and the specifications of the channels considered are expressed in Table I. The simulation considers $M = 256$, $\overline{M} = 32$, subcarrier spacing $\Delta f(= 1/T) = 15kHz$, $P = 1, Q = 3$, $L = \{2,4,8,16\}$ and various QAM modulation such as 4QAM, 16QAM, 64QAM, 128QAM, 256QAM. The channel is considered for EPA, EVA and ETU scenario between SR and the receiver and flat-fading between the transmitter and SR and the noise is AWGN.

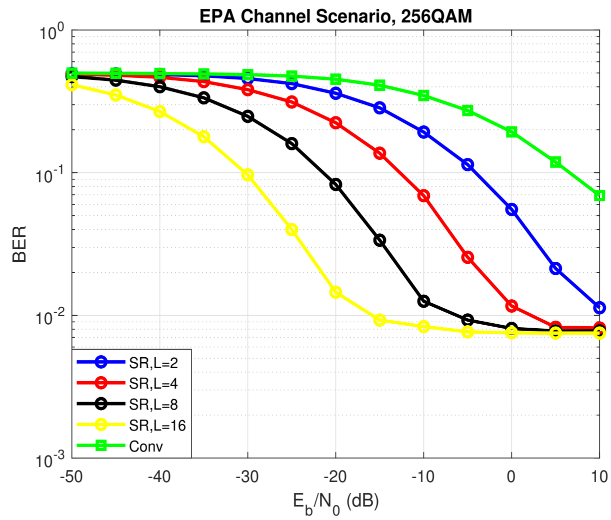


Fig. 9. BER Comparison for different $L$ with EPA Channel, 256QAM modulation.

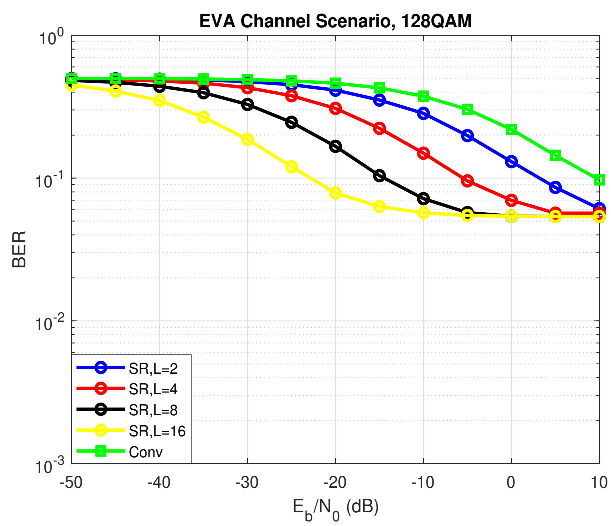


Fig. 10. BER Comparison for different $L$ with EVA Channel, 128QAM modulation.

Figures 7, 8, 9, 10, 11, 12, 13, and 14 depicts the BER performance comparison of the proposed SR assisted

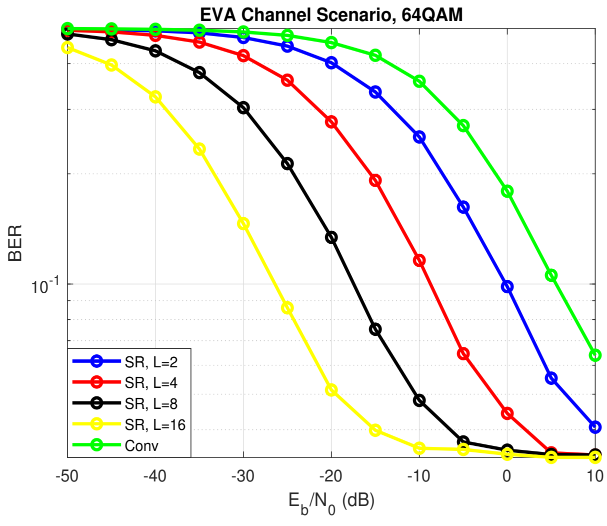


Fig. 11. BER Comparison for different $L$ with EVA Channel, 64QAM modulation.

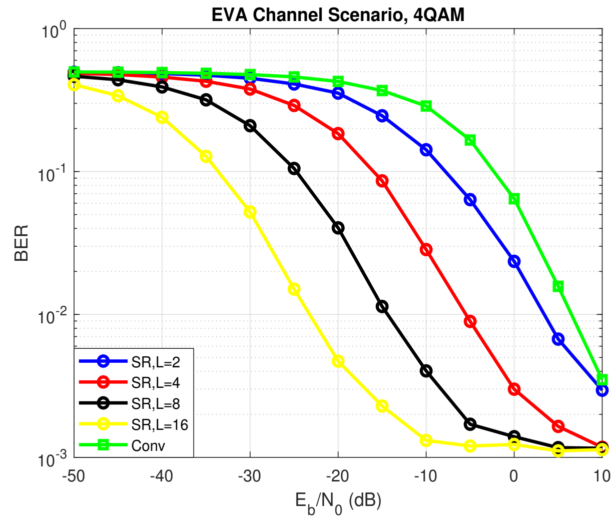


Fig. 12. BER Comparison for different $L$ with EVA Channel, 4QAM modulation.

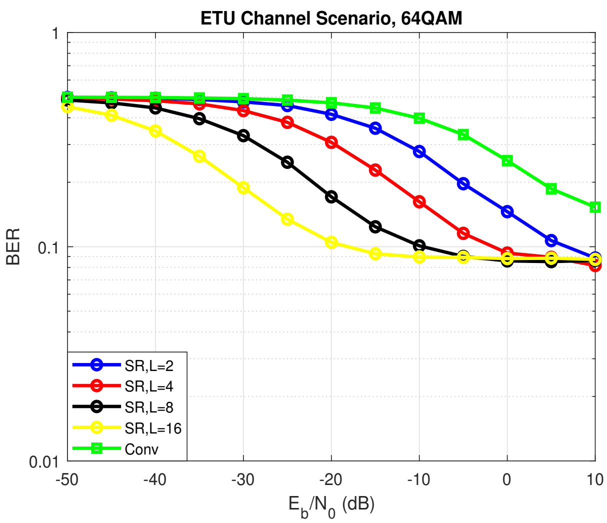


Fig. 13. BER Comparison for different $L$ with ETU Channel, 64QAM modulation.

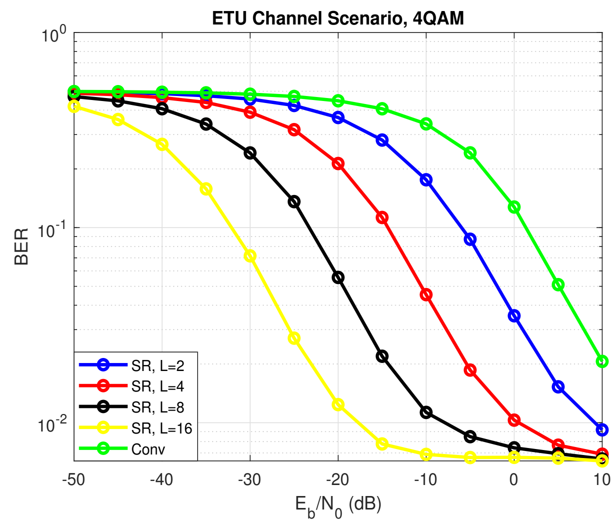


Fig. 14. BER Comparison for different $L$ with ETU Channel, 4QAM modulation.

Alamouti-coded FBMC-OQAM system for $L = \{2, 4, 8, 16\}$ with conventional Alamouti-coded FBMC-OQAM system for 16QAM modulation technique-EPA channel scenario, 64QAM modulation technique-EPA channel scenario, 256QAM modulation technique-EPA channel scenario, 128QAM modulation technique-EVA channel scenario, 64QAM modulation technique-EVA channel scenario, 4QAM modulation technique-EVA channel scenario, 64QAM modulation technique-ETU channel scenario, and 4QAM modulation technique-ETU channel scenario, respectively. The figures show that as the number of reflecting elements $L$ in the SR increases, the BER performance significantly increases. The rise in $L$ leads to an increase in the effective SNR at the receiving antenna, as $\gamma$ is linearly dependent on $L$ (28). As shown in the figure, the BER saturates in Alamouti-coded FBMC systems at high SNR because: 1) the influence of noise in BER reduces at high SNR, 2) in EPA channel scenario, because of multipath propagation, residue interference exists in (24). At higher value of $L$ in SR assistance, the effective SNR increases at a rate of $\gamma^2$; therefore, the noise becomes insignificant comparatively at lower SNR. Thus, the BER saturates at an early SNR for a higher value of $L$. The reflecting elements are termed as almost passive which means that these elements are not processing the incident waves at RF level. They simply reflect the waves introducing appropriate phases, after which the waves become constructive. For this purpose they consume very little amount of power. As $L$ increases, the number of reflected waves constructively added at the receiver increases. Hence, the received signal strength increases which is evident from the figure. For $L \geq 2$, the SR-assisted system performs better than the conventional system for all the range of $E_b/N_0$ considered.

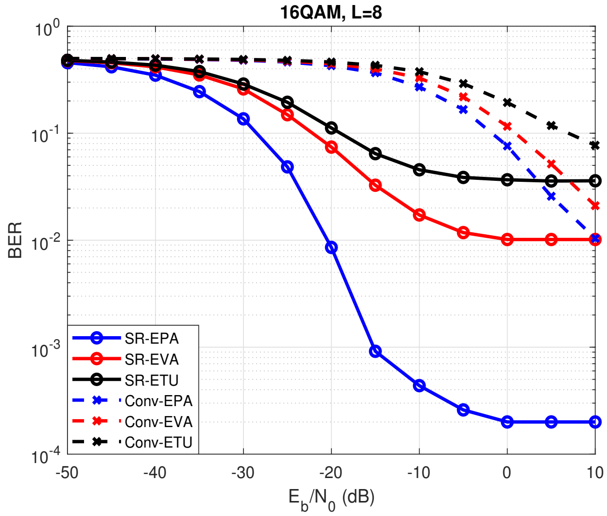


Fig. 15. BER Comparison for 16QAM modulation and $L = 8$ with different Channel.

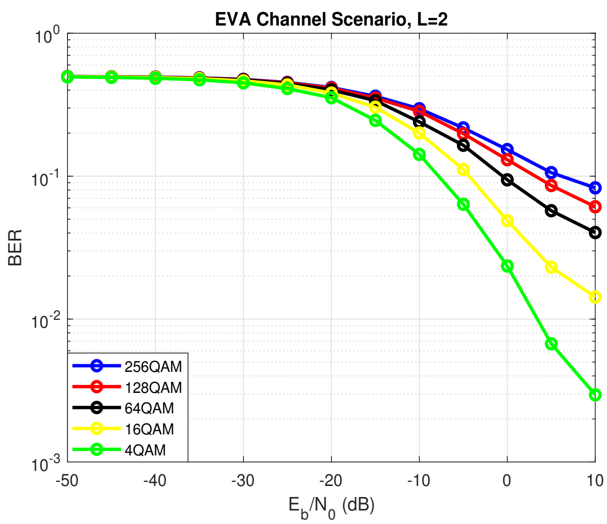


Fig. 16. BER Comparison for EVA Channel scenario and $L = 2$ with different QAM modulation.

Figure 15 depicts the BER performance analysis of the SR assisted Alamouti-coded FBMC-OQAM system for $L = 8$ with conventional Alamouti coded FBMC-OQAM system for 16QAM modulation technique for EPA, EVA and ETU channel scenario. BER performance is the best in EPA than EVA and is worst in ETU channel scenario as anticipated. In all cases the BER performance of the SR-assisted system is better than the conventional system. A comparative analysis of BER is presented in TABLE II for some scenarios.

Similarly, figure 16 depicts the BER performance comparison of the proposed SR assisted Alamouti-coded FBMC-OQAM system for $L = 2$ with conventional Alamouti-coded FBMC-OQAM system for EVA channel scenario. The figure shows that as the QAM modulation increases, the BER performance degrades as the modulation noise increases in higher modulation techniques. The observation from the figures and the table ratifies that the proposed system also performs well in variety of modulation schemes and channel scenario.

## V. CONCLUSION

This article introduces a smart reflector-assisted transmission scheme for Alamouti-coded FBMC-OQAM system in LTE channel scenario. The modulated signal is transmitted to the smart reflector, which changes the phase of the incoming wave to cancel out the channel phases. The reflected wave is transmitted to the channel and then received by the receiver. We evaluated the BER performance of EPA, EVA and ETU channels using modulation techniques including 4QAM, 16QAM, 64QAM, 128QAM, and 256QAM. Our comparison showed that the BER of the proposed scheme is superior than the conventional Alamouti-coded FBMC-OQAM system. The proposed approach is of practical value for future wireless communication.

## VI. AUTHOR CONTRIBUTION

Radhashyam Patra got the idea of incorporating SR-assistance in Alamouti coded FBMC-OQAM system and also did the programming in MATLAB. Arunanshu Mahapatro helped in deriving mathematical equations and overall guidance while preparing the manuscript.

## REFERENCES


[1] A. Osseiran, F. Boccardi, V. Braun, K. Kusume, P. arsch, M. Maternia, O. Queseth, M. Schellmann, H. Schotten, H. Taoka, H. Tullberg, M. A. Uusitalo, B. Timus, and M. allgren, "Scenarios for 5G mobile and wireless communications: the vision of the METIS project," IEEE Commun. Mag., vol. 52, no. 5, pp. 26-35, May 2014.

[2] 3GPP TS 36.201, "LTE physical layer; General description (Release 9)," 3GPP TSG RAN, Tech. Rep. v9.1.0, 2010.

[3] B. Le Floch, M. Alard, and C. Berrou, "Coded ortho gonal frequency division multiplex [TV broad casting]," Proc. IEEE, vol. 83, no. 6, pp. 982-996, Jun. 1995.

[4] P. Siohan, C. Siclet, and N. Lacaille, "Analysis and design of OFDM/OQAM systems based on filterbank theory," IEEE Trans. Signal Process., vol. 50, no. 5, pp. 1170-1183, May 2002.

[5] M. Schellmann, Z. Zhao, H. Lin, P. Siohan, N. Rajatheva, V. Luecken, and A. Ishaque, "FBMC-based air interface for 5G Mobile: Challenges and proposed solutions," in Proc. 9th Int. Conf. Cogn. Radio Oriented Wirel. Networks, no. i. ICST, 2014, pp. 102 - 107.

[6] Patra, R., Mahapatro, A. and Sahu, A.K. (2020), Receiver design for CDMA-FBMC/ OQAM systems. Electron. Lett., 56: 848-851. https://doi.org/10.1049/el.2020.0524

[7] S. E. E. Ayoubi, M. Boldi, I.Bulakci, P. Spapis, M. Schellmann, P. Marsch, M. Siily, J. F. Monserrat, T. Rosowski, G. Zimmermann, I. D. Silva, M. Tesanovic, M. Shariat, and Ahmed M. Ibrahim, "Preliminary Views and Initial Considerations on 5G RAN Architecture and Functional Design," White Pap. METIS II, pp. 1-27, 2016.

[8] A. Viholainen, M. Bellanger, and M. Huchard, "Prototype filter and structure optimization," PHYDYAS, Tech. Rep., 2009.

[9] M. Gharba, R. Legouable, and P. Siohan, "An alternative multiple access technique for the uplink 3GPP/LTE based on OFDM/OQAM," in 2010 7th Int. Symp. Wirel. Commun. Syst. IEEE, Sep. 2010, pp. 941-945.

[10] F. Schaich, J. Vandermot, V. Ringset, H. Rustad, M. Najar, F. Rubio, M. Caus, and Z. Zhipeng, "WiMAX simulation results - Lab setup and measurements," ICT-211887 PHYDYAS Deliv. D9.3, pp. 1-115, 2010.
[11] M. Fuhrwerk, S. Moghaddamnia and J. Peissig, "Scattered Pilot-Based Channel Estimation for Channel Adaptive FBMC-OQAM Systems," in IEEE Transactions on Wireless Communications, vol. 16, no.3, pp. 1687-1702, March 2017, doi: 10.1109/TWC.2017.2651806.
[12] S.M. Alamouti, "A simple transmit diversity technique for wireless communications," IEEE Journal on Selected Areas in Communications, vol. 16, no. 8, pp. 1451-1458, Oct. 1998.
[13] M. Renfors, T. Ihalainen, and T. H. Stitz, "A block-Alamouti technique for filter bank based multicarrier transmission", in Proc. Eur. Wireless Conf., 2010, pp. 10311037.
[14] D. Na and K. Choi, "Intrinsic ICI-Free Alamouti Coded FBMC," in IEEE Communications Letters, vol. 20, no. 10, pp. 1971-1974, Oct. 2016, doi: 10.1109/LCOMM.2016.2593922.
[15] Patra, R., Mahapatro, A. & Choi, K. Orthogonal affine precoding and decoding based channel estimation and data detection in frequency reversed Alamouti coded FBMC-OQAM system. Int. j. inf. tecnol. 16, 1863-1872 (2024). https://doi.org/10.1007/s41870-023-01551-w
[16] E. Basar, "Transmission Through Large Intelligent Surfaces: A New Frontier in Wireless Communications," 2019 European Conference on Net- works and Communications (EuCNC), 2019, pp. 112-117, doi: 10.1109/Eu- CNC.2019.8801961.
[17] M. Di Renzo et al., "Smart radio environments empowered by reconfigurable AI meta-surfaces: An idea whose time has come," EURASIP J. Wireless Commun. Net., vol. 2019, p. 129, May 2019.
[18] Y. Naresh and A. Chockalingam, "On Media-Based Modulation Using RF Mirrors," in IEEE Transactions on Vehicular Technology, vol. 66, no. 6, pp. 4967-4983, June 2017, doi: 10.1109/TVT.2016.2620989.
[19] J. Liu, H. Arslan and L. P. Dunleavy, "Effect of power amplifier impairments in designing OFDM based wireless communication system," 2003 IEEE Topical Conference on Wireless Communication Technology, 2003, pp. 33-34, doi: 10.1109/WCT.2003.1321430.
[20] Yuxiao Yang, Xiaolu Zhang, and Xiaobo Shen, “PAPR Suppression Method for Probability-oriented MP-WFRFT," Engineering Letters, vol. 32, no. 12, pp2362-2370, 2024.
[21] C. Liaskos, S. Nie, A. Tsioliaridou, A. Pitsillides, S. Ioannidis and I. Akyildiz, "A New Wireless Communication Paradigm through Software-Controlled Metasurfaces," in IEEE Communications Magazine, vol. 56, no. 9, pp. 162-169, Sept. 2018, doi: 10.1109/MCOM.2018.1700659.
[22] L. Subrt and P. Pechac, "Controlling propagation environments using intelligent walls," in Proc. 2012 6th European Conf. Antennas Propag. (EU- CAP), Prague, Czech Republic, Mar. 2012, pp. 1-5.
[23] Patra, R. and Mahapatro, A. (2024), RIS-Assisted Propagation Control in CDMA-FBMC-OQAM System. Internet Technology Letters e621. https://doi.org/10.1002/itl2.621.
[24] P. Chen, X. Li, M. Matthaiou and S. Jin, "DRL-Based RIS Phase Shift Design for OFDM Communication Systems," in IEEE Wireless Communications Letters, vol. 12, no. 4, pp. 733-737, April 2023, doi: 10.1109/LWC.2023.3242449.
[25] Liu X, Guo Y. Energy-efficient resource allocation and passive beamforming design for multiuser IRS-aided OFDM SWIPT. Internet Technology Letters. 2023; 6(4):e428. doi: 10.1002/itl2.428
[26] R. Patra and A. Mahapatro, “Reconfigurable Intelligent Surface-based Propagation Control in FBMC/OQAM Systems", JTIT, vol. 95, no. 1, pp. 83-90, Mar. 2024, doi: 10.26636/jtit.2024.1.1326.
[27] 3GPP TS 36.101.“Evolved Universal Terrestrial Radio Access (E-UTRA); User Equipment (UE) Radio Transmission and Reception" 3rd Generation Partnership Project; Technical Specification Group Radio Access Network. https://www.3gpp.org.
[28] 3GPP TS 36.104. “Evolved Universal Terrestrial Radio Access (E-UTRA); Base Station (BS) Radio Transmission and Reception." 3rd Generation Partnership Project; Technical Specification Group Radio Access Network. URL: https://www.3gpp.org.
[29] M. Bellanger, "Specification and design of a prototype filter for filter bank based multicarrier transmission" in Proc. ICASSP, Salt Lake, UT, USA, May 2001, pp. 2417-2420.
[30] Yin-Yin Bao, Yu Liu, Jie-Sheng Wang, and Jia-Xu Liu, “Genetic Algorithm Based on Grid Maps for Solving Robot Path Planning Problem," Engineering Letters, vol. 31, no.4, pp1635-1648, 2023
[31] Y. F. Zhao, Z. Q. Dai, F. Li, X. W. Zhu, and C. X. Ran, “A New Attention-based Neural Network for The Identification of Non-line-of-sight Signals in Data from Global Navigation Satellite Systems," Engineering Letters, vol. 32, no. 10, pp2012-2022, 2024.
[32] Md. Abdul Alim Sheikh, Tanmoy Maity, and Alok Kole, “Deep Learning Approach using Patch-based Deep Belief Network for Road Extraction from Remote Sensing Imagery," IAENG International Journal of Applied Mathematics, vol. 52, no.4, pp760-775, 2022
[33] Favour Femi-Oyewole, Victor Osamor, and Daniel Okunbor,“Ensemble Machine Learning Approach For Identifying Real-Time Threats In Security Operations Center," IAENG International Journal of Computer Science, vol. 51, no. 12, pp2094-2122, 2024.